Acoustic-magnetic Signatures of Vessels

Lukas Schirmer[1], Martin Rosner[2], Moritz Boueke[1], Bastian Kaulen[1], Marco Driesen[1], Christian Kanarski[1], Finn Röhrdanz[1], Konstantinos Karatziotis[1], Frederik Kühne[1], Ralf Burgardt[1], Viktoriia Boichenko[1], Karoline Gussow[1] und Gerhard Schmidt[1]

[1] *Digital Signal Processing and System Theory, Department of Electrical and Information Engineering, Kiel University*
Email: {lusc, mobo, bk, madr, chk, finr, koka, frk, rabu, vik, gssw, gus}@tf.uni-kiel.de
[2] *Wehrtechnische Dienststelle für Schiffe, Marinewaffen, Maritime Technologie und Forschung, 24340 Eckernförde, Germany*

Introduction

Vessels generate various physical signatures while moving through water, including acoustic and magnetic signals, which can either provide valuable information or act as noise sources that interfere with measurements.

The acoustic signature of a vessel is primarily influenced by propeller rotation, cavitation, and mechanical noise, and can be measurable over several kilometers [1]. However, even without propulsion, the acoustic signature may persist in the water for several minutes [2], acting as a temporary noise source in the surrounding environment.

In addition to acoustic noise sources, a vessel also generates a magnetic signature. As a ship moves through water, it generates hydrodynamic turbulence and coherent flow structures, collectively referred to as the wake flow [3]. In particular, within conductive fluids such as seawater, these flow structures are assumed to produce measurable magnetic signals over longer distances and timescales [4]. The magnetic field strength and the spectral characteristics of these signals depend on various factors, including flow dynamics, vessel speed, and the electrical properties of the water.

While acoustic signatures have been extensively studied, the short- and long-term measurability of magnetic wakes remains an open research question. In particular, it is still unclear how long these magnetic effects persist in the water, at what intensity they can be measured, and which physical mechanisms govern their behavior. This work aims to identify the various sources of magnetic signals and analyze their characteristic features. Furthermore, an initial simulation approach is presented to model the magnetic signature of a Kelvin wave pattern and propeller-induced vortices.

Signal Modeling

When a ship is in motion and driven by a propeller, it initially exhibits a fundamental frequency referred to as the rotational frequency f_r. The blades of the propeller generate harmonic frequency components that are integer multiples of the rotational frequency. This so-called Blade Passing Frequency (BPF) is directly related to the rotational frequency and is given by:

$$f_{\mathrm{BPF}} = N \cdot f_r, \tag{1}$$

where N denotes the number of propeller blades. The modulation of the signal can be expressed as a sum of harmonic components [5]:

$$s(t) = \sum_{k=0}^{K-1} A_k \sin(2\pi k f_{\mathrm{BPF}} t + \phi_k). \tag{2}$$

Here, K represents the number of harmonic components, A_k is the amplitude of the k-th harmonic, k is the harmonic index, and ϕ_k denotes the phase offset of the individual components.

Cavitation refers to the expansion and collapse of bubbles in a liquid due to local pressure drops [1]. In the case of ship propellers, cavitation typically occurs at the blade tips and on the suction side of the blades when the local pressure falls below the vapor pressure of water. The resulting cavitation bubbles are unstable and collapse rapidly, producing local pressure shocks that can be perceived both acoustically and magnetically. The cavitation signal $v_c(t)$ can be considered as carrier signal that modulates the fundamental signal $s(t)$ via amplitude modulation:

$$\hat{s}(t) = \big[1 + s(t)\big] v_c(t) + v_a(t). \tag{3}$$

Here, $v_a(t)$ summarizes all additional noise sources, such as engine noise and environmental background noise.

To model the magnetic signal, it is assumed that a ferromagnetic propeller produces periodic disturbances in the magnetic field. These are caused by the rotation of the blades and can be attributed primarily to the BPF [6]. Such a source can be represented as a time-dependent magnetic dipole moment [6]:

$$\boldsymbol{m}(t) = m_0 \cos(\omega t)\boldsymbol{e}_x + m_0 \sin(\omega t)\boldsymbol{e}_y, \tag{4}$$

where ω is the angular frequency and $\boldsymbol{e}$ denotes a unit vector. This model leads to a magnetic field signal with a fundamental component at f_{BPF} and higher harmonics. The amplitude of the field depends on the remanent magnetization of the propeller material.
To estimate the induced magnetic field, this work focuses on the principles of magnetohydrodynamics (MHDs). MHDs describe the induction of electrical currents due to the motion of a conductive fluid, such as seawater, and the resulting magnetic field [3]. The derivation of

the modified induction equation (6) is omitted in this work and instead referenced to [7, 8, 9]. Equation (6) describes the interaction between the induced field $\boldsymbol{b}$ and the earth's magnetic field $\boldsymbol{B_0}$, where the total field results in:

$$\boldsymbol{B} = \boldsymbol{B_0} + \boldsymbol{b}. \tag{5}$$

The modified induction equation is defined as:

$$\frac{\partial \boldsymbol{b}}{\partial t} + (\boldsymbol{v}\cdot\nabla)\boldsymbol{b} = ((\boldsymbol{B_0} + \boldsymbol{b})\cdot\nabla)\boldsymbol{v} + \frac{1}{\mu_m \sigma}\nabla^2 \boldsymbol{b} - (\boldsymbol{v}\cdot\nabla)\boldsymbol{B_0}. \tag{6}$$

The term $(\boldsymbol{v}\cdot\nabla)\boldsymbol{b}$ accounts for the influence of the flow on the magnetic field. Here, $\boldsymbol{v}$ represents the flow velocity, σ the electrical conductivity of water, and μ_m the magnetic permeability. Assuming the earth's magnetic field is locally known and static, the equation needs only to be solved for the induced magnetic field. This allows the simplification:

$$(\boldsymbol{v}\cdot\nabla)\boldsymbol{B_0} = \boldsymbol{0}. \tag{7}$$

Moreover, assuming that $\boldsymbol{b}$ is much smaller than $\boldsymbol{B_0}$, equation (6) can be linearized as:

$$\frac{\partial \boldsymbol{b}}{\partial t} + (\boldsymbol{v}\cdot\nabla)\boldsymbol{b} = (\boldsymbol{B_0}\cdot\nabla)\boldsymbol{v} + \frac{1}{\mu_m \sigma}\nabla^2 \boldsymbol{b}. \tag{8}$$

It should be noted that equation (8) represents a lower bound of the induced magnetic field. A more comprehensive description would require consideration of additional factors such as the ship's material composition, salinity of the water, and the orientation of the wake relative to the earth's magnetic field.

Kelvin Wave Patterns

The displacement of water by the ship's hull generates a pressure-induced flow that propagates as a Kelvin wave pattern. These long-wavelength flows can influence the local magnetic field when coupled with electrically conductive water and lead to electromagnetic induction in the presence of velocity gradients [7].

For modeling the Kelvin wave pattern, it is assumed that the ship's motion can be approximated by a source dipole, consisting of a source at the bow and a sink at the stern [10]. The surface wave generated by this source dipole, which describes the disturbance of the free surface as a function of the coordinates x and y, is denoted as $\zeta(x, y)$.

The surface elevation as derived in [4, 11, 12] is given by:

$$\zeta(x,y) = \underbrace{\frac{\mu F^2}{\pi^2}\int_0^{\pi/2}\cos\theta\int_0^{\infty}\frac{k^2 e^{-k|x|}\cos(ky\sin\theta)g(k,\theta)}{F^4k^2+\cos^2\theta}\,dkd\theta}_{\text{Surface wave}} \underbrace{-\frac{\mu H(x)}{\pi}\int_{-\infty}^{\infty}\xi^2 e^{-F^2\xi^2}\sin(x\xi)\cos(y\xi\lambda)\,d\lambda}_{\text{Local disturbance}}. \tag{9}$$

The first term of the integral describes the free surface wave generated by the ship, which propagates across the entire water surface. The second term represents a localized pressure disturbance at the free surface, directly caused by the submerged bow of the vessel [11]. The simulated surface profile of an approximated ship wake is shown in Fig. 1. In Fig. 1 the maxima of the wave are

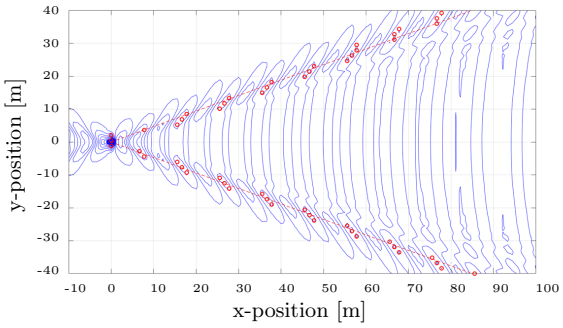

Figure 1: Kelvin wave pattern as contour plot.

marked in red and the typical propagation angle of 19.47° is marked with the dashed lines. An important parameter influencing the wake is the dimensionless Froude number F, which describes the ratio of inertial to gravitational forces in the flow [4]. It is defined as:

$$F = \frac{U}{\sqrt{gH}}, \tag{10}$$

where H is the vessel's draft and U its velocity. In general, $F < 1$ corresponds to displacement mode, $F \approx 1$ to transitional motion, and $F > 1$ to planing motion. The wave amplitude is described by the coefficient κ with units of m^4/s. The corresponding dimensionless wave efficiency μ is given by:

$$\mu = \frac{\kappa}{UH^3}. \tag{11}$$

Higher values of μ lead to larger wave amplitudes generated by the hull. The simulation assumes planing motion with a Froude number of $F = 1.5$, a vessel speed of $U = 15\,\mathrm{m/s}$, and a wave efficiency of $\mu = 0.8$. For reference, this corresponds to the profile of a dynamically supported vessel [3]. The wave height of the propagation is shown in Fig. 2.

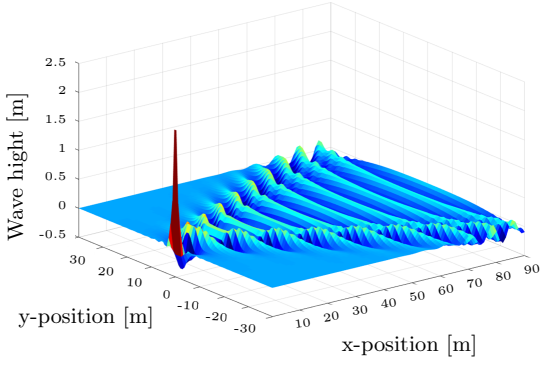

Figure 2: Simulated wave elevation of the ship wake.

The relationship between the surface profile of the Kelvin wave and the resulting magnetic field is established through the velocity components of the flow-induced motion, which are described by the gradients of the velocity potential [3, 13]:

$$v_x = \frac{\partial \phi}{\partial x}, \quad v_y = \frac{\partial \phi}{\partial y}. \tag{12}$$

Only the horizontal velocity components (x, y) are considered here, since the induced magnetic field is analyzed with respect to its vertical z component.
The velocity potential $\phi(x, y)$ is defined as:

$$\phi(x, y) = -\frac{g}{U} \int_{-\infty}^{\infty} \zeta(x, y)\, dx. \tag{13}$$

By inserting equation (12) into the modified induction equation (6), the induced magnetic field caused by the Kelvin waves can be computed.

For the simulation, an Earth magnetic field of $B_z = 50\,\mu\text{T}$ was assumed [4], and the resulting magnetic field is illustrated in Fig. 3. The simulation results indicate a

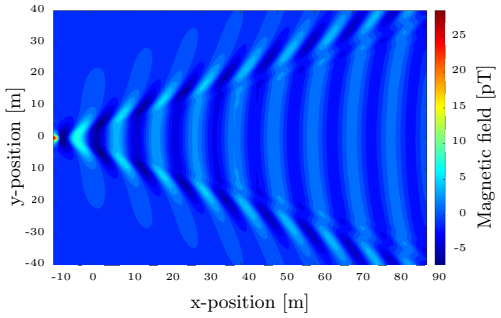

Figure 3: Intensity of the resulting magnetic field in the B_z component.

magnetic field strength in the pT regime. These values are consistent with the results reported in [4, 7, 12], although [7] reports higher field strengths in the nT range under conditions of reduced ocean depth.

The findings indicate that the induced magnetic field persists over extended distances in water before gradually attenuating due to damping mechanisms. It is also assumed that the Kelvin wave pattern may be measurable as a low-frequency pressure variation using fiber optic hydrophones [14], suggesting potential relevance for acoustic signature analysis as well.

Propeller-induced Wake

The rotation of a propeller generates a characteristic flow structure that can be broadly divided into a tip vortex and a hub vortex. The tip vortex is caused by the pressure difference between the upper and lower surfaces of the propeller blades. In contrast, the hub vortex essentially represents the central wake flow behind the propeller and resembles a jet stream generated by the propulsion system.

These vortex structures are highly dependent on various parameters such as propeller geometry, rotational speed, inflow conditions, and the surrounding environment and remain stable only for a limited time [13]. For this reason, the wake flow in this study is simplified and modeled as a combination of large-scale structures, high-energy flow zones, and turbulent fluctuations. To describe such structures, the Large Eddy Simulation (LES) model is well suited [15]. In LES, the Navier–Stokes equations are spatially filtered to separate large and small eddies. The advantage of this approach is that only the large eddies need to be resolved explicitly, while the smaller scales are approximated using a Subgrid-Scale (SGS) model. The filtered Navier–Stokes equation is given by

$$\frac{\partial \bar{u}_i}{\partial t} + \frac{\partial (\bar{u}_i \bar{u}_j)}{\partial x_j} = -\frac{1}{\rho} \frac{\partial \bar{p}}{\partial x_i} + \nu \frac{\partial^2 \bar{u} i}{\partial x_j \partial x_j} - \frac{\partial \tau_{ij}}{\partial x_j}. \tag{14}$$

The term τ_{ij} denotes the subgrid-scale (SGS) tensor, which represents the effect of the unresolved small-scale turbulence. In this work, a simplified velocity profile is used, and it is only noted that a more detailed modeling of turbulent flow is possible using equation (14) [9]. By inserting the velocity components into the MHD equation (6), the magnetic signature induced by the wake flow can be simulated. The results of this simplified model are shown in Fig. 4, based on an assumed flow velocity of $U = 10\,\text{m/s}$ and a ship width of 10 m. The calculation

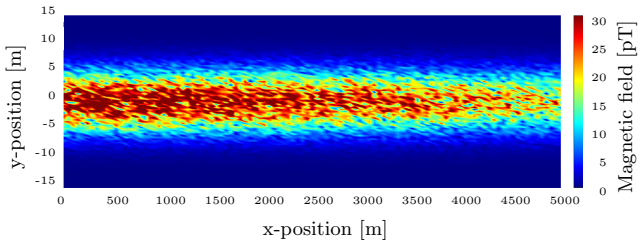

Figure 4: Propeller-induced wake at a ship speed of 10 m/s and a vessel width of 10 m.

of absolute magnetic field strength follows methodologies described in the literature [8, 9, 15, 16]. The results suggest that the magnetic field induced by the approximated wake flow may remain measurable in water over extended periods. However, the actual persistence strongly depends on the specific flow characteristics and their interaction with the earth's magnetic field. Due to model simplifications, localized effects such as induced secondary flows or small-scale vortex shedding cannot be resolved.
Consistent with the literature, the magnetic field may remain measurable for up to one hour. The field intensity also depends on the alignment of the wake flow relative to the earth's magnetic field depending on the orientation, the field may be either amplified or attenuated. It should be emphasized that the simulation represents a simplified model of the wake flow. While major flow features are captured, finer details such as the direct propeller jet and small-scale vortex interactions are not explicitly resolved. A more accurate representation would require high-resolution simulations that include the detailed propeller geometry. Such simulations e.g., using

OpenFOAM[1] entail significantly higher computational cost.

As mentioned previously, the effects of cavitation on the magnetic signature must be considered separately. The implosion of cavitation bubbles is associated with extremely high temperatures and pressures, which can lead to ionization of the fluid inside the bubbles [1, 17]. The resulting charged particles move at high velocities for a brief moment during the collapse, generating a high-frequency magnetic field [18, 19]. However, such magnetic signals are expected to be very short-lived [19], and both their frequency and intensity are difficult to measure experimentally [20].

Regarding the acoustic signature, it is assumed that the noise generated by bubbles and turbulence is initially characteristic, but becomes indistinguishable from ambient background noise within a few minutes.

Discussion

The simulations of Kelvin waves and propeller-induced wake flows demonstrate that magnetic effects in the range of several pT can develop and persist in water over a significant period of time. This indicates that such signals can act as low-frequency magnetic noise sources. It should also be mentioned that the calculation of the induced magnetic field is based on a simplified model. In reality it is expected that other factors will strengthen the field. Sensors such as fluxgates or optically pumped magnetometers, which offer sensitivities in the picotesla range, may be capable of experimentally detecting these signatures.

The next logical step toward validating the theoretical predictions is an experimental confirmation of the simulation results. For this purpose, an experimental set-up was developed to mimic the turbulent flows. Furthermore, a self-sufficient measuring unit was designed, which is to be used for real-time measurement.

References

[1] Hashmi, Muhammad Abdur Rehman, and Rana Hammad Raza. "Novel DEMON spectra analysis techniques and empirical knowledge based reference criterion for acoustic signal classification." Journal of Electrical Engineering and Technology 18.1 (2023): 561-578.

[2] Smith, Tom A., and Jake Rigby. "Underwater radiated noise from marine vessels: A review of noise reduction methods and technology." Ocean Engineering 266 (2022): 112863

[3] Newman, John Nicholas. "Marine hydrodynamics." The MIT press, (2018).

[4] Fallah, Mohammad-Amir, and Mehdi Monemi. "Optimal magnetic wake detection in finite depth water." Prog. Electromagn. Res. M 106 (2021): 25-34.

[5] Hodges, Richard P. "Underwater acoustics: Analysis, design and performance of sonar". John Wiley & Sons, (2011).

[6] Song, Shuang, et al. "An electromagnetic localization and orientation method based on rotating magnetic dipole." IEEE Transactions on Magnetics 49.3 (2012): 1274-1277.

[7] Fallah, M. Amir, and Habibolah Abiri. "Multi-sensor approach in vessel magnetic wake imaging." Wave Motion 51.1 (2014): 60-76.

[8] Chen, Qing, et al. " Evolutions of hydrodynamic and electromagnetic wakes induced by underwater vehicles." Applied Ocean Research 140 (2023): 103750.

[9] Matt, Silvia, et al. "Fine-scale features on the sea surface in SAR satellite imagery–Part 2: Numerical modeling." Ocean Science 10.3 (2014): 427-438.

[10] Göteman, Malin, et al. "Fluid dynamics and wave-structure interactions." Modelling and Optimization of Wave Energy Converters. CRC Press, 2022. 61-96

[11] Pethiyagoda, Ravindra, Scott W. McCue, and Timothy J. Moroney. "What is the apparent angle of a Kelvin ship wave pattern?." Journal of fluid mechanics 758 (2014): 468-485.

[12] Xue, Fuduo, et al. "Wake features of moving submerged bodies and motion state inversion of submarines." IEEE Access 8 (2020): 12713-12724.

[13] Dingemans, Maarten W. "Water wave propagation over uneven bottoms (in 2 parts)." Vol. 13. World Scientific, (1997).

[14] Luo, Zhengchun, et al. "Low-frequency fiber optic hydrophone based on weak value amplification." Optics Express 28.18 (2020): 25935-25948.

[15] Huang, Bo, et al. "Mechanism and evolution of the wake magnetic field generated by underwater vehicles." Ocean Engineering 303 (2024): 117779.

[16] Wang, Lianzhou, et al. "The dynamic characteristics in the wake systems of a propeller operating under different loading conditions." Ocean Engineering 286 (2023): 115518.

[17] Flannigan, David J., and Kenneth S. Suslick. "Inertially confined plasma in an imploding bubble." Nature Physics 6.8 (2010): 598-601.

[18] Arran, Christopher, et al. "Measurement of magnetic cavitation driven by heat flow in a plasma." Physical Review Letters 131.1 (2023): 015101.

[19] Prevenslik, T. V. "Magnetic fields in the Plank theory of sonoluminescence." Nuclear Science and Techniques, 9(4), (1998). 221–226.

[20] Pochylý, F., and S. Fialová. "The cavitation effect on the electromagnetic field." Recent Advances in Mechatronics. Berlin, Heidelberg: Springer Berlin Heidelberg, (2010). 109-114.

[1] https://www.openfoam.com